Thermal Stability of Au Nanoparticles in O_2 and Air on Fully Oxidized TiO_2(110) Substrates at Elevated Pressures. An AFM/XPS Study of Au/TiO_2 Model Systems

S. Kielbassa, M. Kinne, and R. J. Behm*

Department Surface Chemistry and Catalysis, University of Ulm, D-89069 Ulm, Germany

Received: April 2, 2004; In Final Form: August 6, 2004

The thermal stability of gold nanoparticles (2.5−4 nm diameter) on fully stoichiometric TiO_2(110) rutile substrates in an O_2 atmosphere and in air at up to ambient pressure, and for comparison under ultrahigh-vacuum (UHV) conditions, was investigated by atomic force microscopy (AFM) and X-ray photoelectron spectroscopy (XPS). Substrate material and annealing parameters were chosen similar to those used for the pretreatment of realistic disperse Au/TiO_2 catalysts. Under UHV conditions, the particles are rather stable even after annealing at 400 °C, and only minor changes in the particle size are detected after annealing at 500 °C. In 50 mbar O_2, the particles are relatively stable at room temperature but grow significantly after annealing to 400 °C. In air, particle growth starts already at room temperature, accompanied by the formation of Au−OH species. The relevance of these results for the understanding of the pretreatment of disperse Au/TiO_2 catalysts is discussed.

1. Introduction

Metal oxide supported Au catalysts, in particular Au/Fe_2O_3 and Au/TiO_2 catalysts, have attracted considerable interest over the last years because of their high activity for low-temperature oxidation and hydrogenation reactions.[1−3] Despite numerous studies important details of the reaction mechanism, in particular the nature of the considerable particle size effects reported in some studies[4] and the mechanism of the O_2 activation, have not yet been resolved. One of the main problems in these mechanistic studies was the ill-defined microscopic structure of the support material and in particular of the interface between support and Au nanoparticles.

Better access to these questions is expected from model studies using well-defined model systems with Au nanoparticles deposited on planar metal oxide substrates[5−21] or metal oxide thin films.[22−25] Because of the pronounced particle size effects for the catalytic activity mentioned above, with particle sizes around 2.5−3.5 nm for the most active Au particles,[4,7,17] the main interest in these model studies concentrated on the stability and activity of the Au nanoparticles on these model systems under different conditions, in particular during catalyst pretreatment and under reaction conditions. Focusing on the former, practically no data are available on the stability of these model systems under conditions close to those commonly applied during pretreatment of realistic supported Au catalysts. Though high surface area catalysts mostly undergo an oxidative treatment before catalytic applications, commonly by calcining in air at 200−400 °C,[2,26] the preparation of the model systems generally involves high-temperature annealing of the TiO_2 substrates under ultrahigh vacuum (UHV) conditions or in a low-pressure O_2 atmosphere (10^{-6} mbar range),[27] which is known to lead to a considerable loss of surface oxygen.[21,28,29] As a basis for further studies on the chemical and catalytic properties of well-defined Au/TiO_2 model systems we investigated the stability of the Au nanoparticles under conditions typical for catalyst pretreatment, upon calcination in air (1 bar) or upon annealing in 50 mbar O_2, following the density and size of the Au nanoparticles and the chemical composition of the Au/TiO_2(110) surface by atomic force microscopy (AFM) and X-ray photoelectron spectroscopy (XPS). To separate thermal and chemical effects, similar measurements were performed for annealing under UHV conditions and for room-temperature exposure to O_2 or air. In these measurements we used fully stoichiometric TiO_2(110) substrates, similar to the situation for realistic catalyst pretreatment, to avoid effects caused by the partial reduction of the TiO_2(110) substrates prepared by standard UHV procedures. Effects of the oxidation state of the substrate on the particle stability had indeed been reported for O_2 exposure of Ag nanoparticles on a reduced or surface-reoxidized TiO_2(110) substrate.[10] Finally we will discuss the relevance of the data obtained here for the understanding of the pretreatment of disperse supported Au/TiO_2 catalysts and of the influence of the pretreatment procedure on the subsequent catalyst deactivation during CO oxidation.

2. Experimental Section

The experiments were performed in an ultrahigh vacuum (UHV) system equipped with a home-built AFM with a laser-beam deflection system (maximum scan range 1 μm × 1 μm),[30] facilities for sample preparation and characterization such as XPS (Specs EA 200), an argon ion gun, and a Au evaporation source. A high-pressure cell, which was attached to the UHV chamber via a gate valve, allowed sample processing at pressures up to atmospheric pressure and to introduce the sample from air via a load lock. In the UHV chamber the sample could be heated by a tungsten filament, in the high-pressure cell it was heated by a boron nitride ceramics heater. The sample temperature was determined via thermocouples connected to the heater button near the sample. During annealing, the temperature was held constant with a variation of ±5 °C.

To avoid displacement of the Au nanoparticles by the AFM tip, the AFM measurements were performed in the attractive noncontact mode (nc-mode), which was tested to have no effect on the Au particle distribution. XP spectra were obtained using

* Corresponding author. E-mail: juergen.behm@chemie.uni-ulm.de.

10.1021/jp048547d CCC: $27.50
Published on Web 11/16/2004

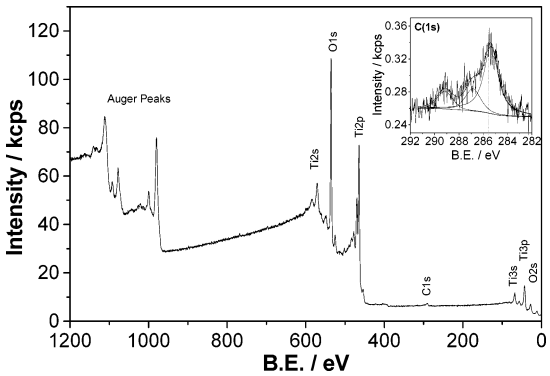

Figure 1. Survey XP-spectrum of a freshly prepared, fully stoichiometric TiO_2(110) surface. The inset shows a high-resolution scan of the C(1s) region.

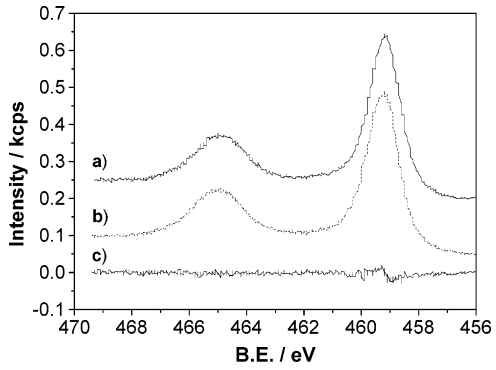

Figure 2. XP-spectrum of the Ti(2p) region of a freshly prepared, fully stoichiometric TiO_2(110) sample (a) before and (b) after annealing to 600 °C in UHV. The difference (a) − (b) is shown in (c).

Al Kα radiation at normal emission. Due to the sample holder required for the AFM measurements the emission angle was limited to rather small emission angles measured versus the surface normal.

The TiO_2(110) rutile samples (one side polished, tolerance of the surface orientation <0.5°) were purchased from TBL Kelpin (Germany). Prior to the experiments the samples were cleaned in acetone (5 min in a supersonic bath), in a H_2O_2/H_2SO_4 mixture (1:1) and in Millipore water, and finally calcined for 1−2 h in an oven in air at 900 °C. Subsequently, the samples were cooled in air and introduced into the UHV. To remove residual adsorbates and volatile contaminants, they were finally annealed for 5 min at 250 °C in 50 mbar O_2 and then cooled in UHV. Au deposition on the freshly prepared substrates was performed from a home-built evaporator, with the sample at room temperature. Nominal Au coverages were calculated from the evaporation time at a calibrated Au flux (ca. 2 monolayers (ML) Au/min), and then cross checked by AFM and XPS. XPS based coverages were determined following the procedure described in.[31,32] Particle densities were averaged from several images at different sample locations. Deviations between particle densities in different images are below 5%. In addition, a constant, systematic deviation between coverages derived from AFM images and those determined from the deposition time of up to 25% is possible. After the experiments Au deposits were removed by cleaning in acetone in a supersonic bath and polishing them with a kimwipe.

3. Results and Discussion

3.1. Clean TiO_2 Substrate. First the topography and the chemical surface composition of the freshly cleaned TiO_2 samples were examined by XPS and AFM. On the basis of the XPS data (a survey XP spectrum of the sample is shown in Figure 1) the surface is very clean except for trace impurities of carbon (2% ± 0.5%). From their binding energy (BE) of 285.3 and 289.1 eV (see inset in Figure 1) we attributed them to adsorbed hydrocarbons and carbonates, which were presumably picked up during the transport through air or produced during the low-temperature annealing process. The atomic sensitivity factor (ASF) corrected O(1s) and Ti(2p) intensities give an O:Ti ratio of 2.3 ± 0.1, similar to a previous report for a fully oxidized TiO_2 substrate.[33] The higher amount of oxygen is due to oxygen-containing species adsorbed on the surface, mainly H_2O/OH species. Detailed spectra of the Ti(2p) peak show no detectable contributions of partly reduced Ti^{3+} or Ti^{2+} species, supporting the above conclusion of a fully oxidized, stoichiometric surface (see Figure 2). (A simple simulation of a Ti(2p) spectrum using the Ti^{4+} and Ti^{3+}(2p) peaks at 459.2 and 457.2 eV (2 eV below the Ti^{4+} peak,[34] respectively, showed that 5% Ti^{3+} can easily be detected in the spectrum at present resolution.) The surface remains free of any detectable reduced Ti species even after 60 min annealing at 600 °C in UHV. Large-area AFM images show that the surface of the calcined samples consists of extended flat terraces with a width of 100−200 nm, which are separated by steps of 0.33 ± 0.01 nm height (see Figure 3). The step height corresponds to monolayer steps on TiO_2(110).

The well ordered step-terrace morphology found on these surfaces differs distinctly from that of TiO_2 surfaces prepared for STM studies. The latter surfaces are commonly prepared by sample annealing in a vacuum at elevated temperatures and/or cycles of Ar^+-sputtering and subsequent annealing, either in a vacuum[6,21,28,29,35−37] or in a O_2 atmosphere, but at much lower pressures than used here, typically at 10^{-6} mbar.[27] Surfaces as highly ordered as those produced in our experiments by annealing in air can only be obtained by vacuum annealing if temperatures over 900 °C are used.[21,27,37] This results, however, in a higher degree of reduction of the surface and an oxygen deficient (1 × 2) reconstruction.

The surface structures obtained this way are highly reproducible. Variation of the annealing temperature between 900 and 1050 °C and the annealing time between 2 and 12 h results in comparable surface topographies. It was found, however, that longer annealing times and/or higher temperatures may lead to segregation of Ca impurities to the surface, as has been reported previously after high-temperature annealing in a vacuum.[38,39]

3.2. Growth of Au Nanoparticles. The distribution, mean particle size, and particle size distribution of Au nanoparticles resulting upon Au deposition on the fully oxidized TiO_2(110) substrates was investigated for Au/TiO_2 model systems with nominal Au coverages of 0.2, 0.3, 0.45, and 1.0 monolyaer (ML), respectively. After Au deposition on the TiO_2 substrates held at room temperature we find the surfaces covered with a high density of Au nanoparticles, which are randomly distributed over the surface (see Figure 4a, c, e). Hence, under these conditions Au growth is dominated by homogeneous nucleation, no favored nucleation sites can be discovered. Evaluation of these and other AFM images of the respective surfaces results in particle densities of 3.9×10^{12}, 4.1×10^{12}, 5.8×10^{12}, and 4.1×10^{12} cm^{-2}. The height distribution (see Figure 4b,d,f) was obtained by measuring several hundred gold particles separately at different locations of the sample. On the samples with very high particle distribution, this might be critical because tip convolution effects could make it difficult to see always the correct height, but our results are in good agreement with the literature (see below). Most of the Au nanoparticles consist of

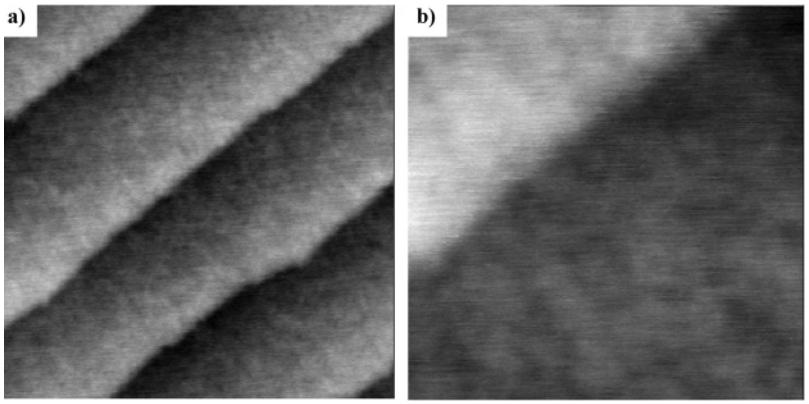

Figure 3. nc-AFM images of a freshly prepared, fully oxidized TiO_2(110) surface: (a) 800 nm × 800 nm; (b) 200 nm × 200 nm.

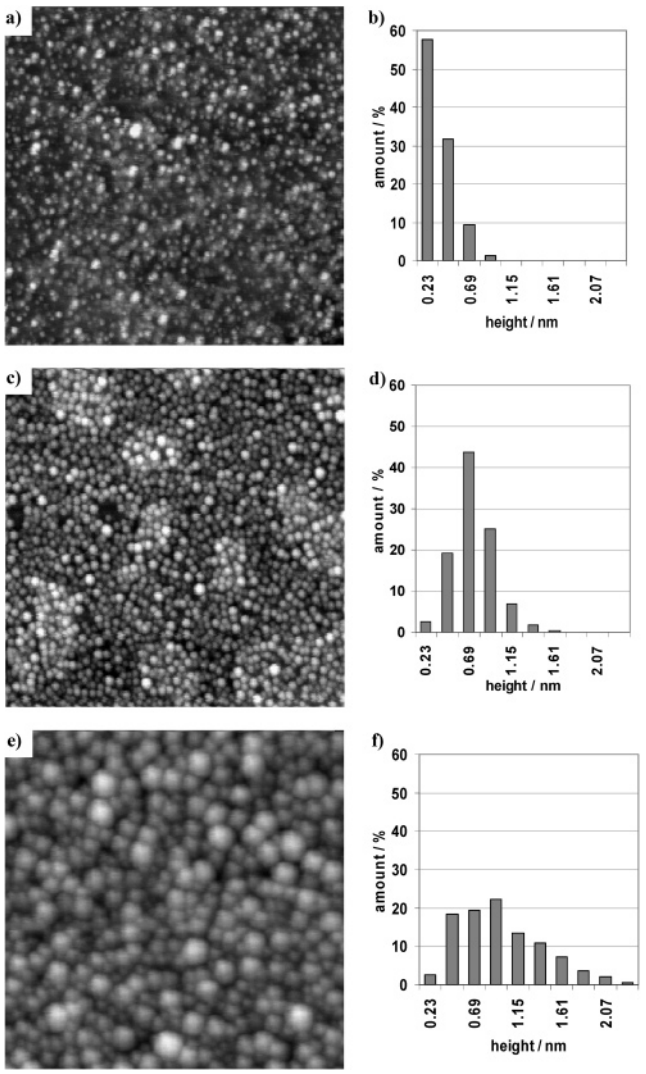

Figure 4. nc-AFM images (a, c, e) of Au/TiO_2(110) samples and the corresponding particle height distributions (b, d, f) after evaporating (a, b) 0.2 ML, (c, d) 0.45 ML Au, and (e, f) 1.0 ML Au on fully oxidized rutile TiO_2(110) substrates (175 nm × 175 nm, 160 nm × 160 nm, and 150 nm × 150 nm).

two-dimensional (2D) monolayer Au islands for the lowest coverage; a height of 0.23 nm corresponds to the height of a Au(111) layer, the reported orientation of the Au islands parallel to the surface.[13,40] Quasi three-dimensional (3D) particles containing two or more Au layers (multilayer islands) are observed for the 1 ML Au covered sample. The particle diameters were estimated indirectly because the apparent diameter of the imaged particles is much larger than in reality due to tip effects, calculating the mean particle diameter from the Au coverages using the mean height of the nanoparticles (h) and the particle density measured from AFM images. For this calculation we assumed spherical segment shaped particles, which is justified on the basis of previous reports of hemispherical particles with larger diameter than height for particles exceeding 5 nm size, and significantly flatter particle shapes for smaller particles.[13] The Au(4f) BE was found to be 84.4 eV for the low coverage and around 84.0 eV for the 1 ML Au covered sample. The latter is identical to the value of 84.0 eV reported for bulk Au.[41] The higher BE value of the low coverage sample is commonly explained by final state particle size effects, which shift the binding energy of the Au electrons to higher values for very small particles.[18,42,43] In the present case, also chemical effects, resulting from the interaction of the Au monolayer islands with the TiO_2 substrate, may contribute.[5]

The general growth behavior is in good agreement with that determined in previous STM or ion scattering (LEIS)/XPS studies on reduced TiO_2(110) single crystals[6−8,10,13,14,17] and thin films.[25] Typical particle densities derived in or from data in those studies are listed in Table 3. The growth of 2D particles is kinetically favored until a certain critical coverage Θ_C is reached, after which a 3D growth starts. The value of Θ_C depends strongly on the surface defect density and temperature and lies typically in the low submonolayer region (0.08−0.2 ML Au).[13]

3.3. Stability of Au/TiO_2 Model Catalysts. Modifications in the surface morphology and the thermal stability of Au/TiO_2 model catalysts were examined using 0.2 ML Au containing samples (small Au clusters are known to have a higher mobility and catalytic activity than the larger ones formed at higher coverages[6,7,10]) upon annealing at 400 and 500 °C under UHV conditions, and after reactive annealing at 400 °C in 50 mbar O_2 and in air (1000 mbar) for 30 min. Furthermore, the stability of 0.1 ML Au covered samples was tested after long-term exposure (up to 72 h) to O_2 (50 mbar) and to air (1 bar) at room temperature.

As can be seen in Figure 5 and Table 1, the Au particles are very stable under UHV conditions. Only minor changes could be observed in the particle density and in the mean particle height and diameter (3.8×10^{12} cm^{-2}, 0.42 nm, 2.6 nm) upon annealing at 400 °C. Correspondingly, the Au(4f) peak intensity did not change, and the Au(4f) BE (84.3 eV) was almost constant (shift: −0.1 eV). Annealing a second sample to 500 °C, however, caused significant changes compared to the sample measured after the evaporation. The density of the Au particles (3.3×10^{12} cm^{-2}) decreased clearly, and also their height

TABLE 1: Change in Density, Mean Height, and Mean Width of the Au Nanoparticles and of the Au(4f) Peak Position and Relative Intensity during Annealing in Different Atmospheres[a]

sample	coverage (ML)	particle density (cm^{-2})	mean height (nm)	mean width (nm)	BE (eV) Au(4f)	rel intensity Au(4f)/Ti(2p)
after evaporation	0.2	$3.9 \times 10^{12} \pm 0.3 \times 10^{12}$	0.35	3.0	84.4	0.15
after evaporation	0.45	$5.8 \times 10^{12} \pm 0.2 \times 10^{12}$	0.74	2.4	84.4	0.25
after evaporation	1.0	$4.1 \times 10^{12} \pm 0.3 \times 10^{12}$	0.93	3.8	84.0	0.47
after 30 min 400 °C in UHV	0.2	$3.8 \times 10^{12} \pm 0.1 \times 10^{12}$	0.42	2.6	84.3	0.15
after 30 min 500 °C in UHV	0.2	$3.3 \times 10^{12} \pm 0.2 \times 10^{12}$	0.47	2.7	84.1	0.13
after 2/15.5 h in O_2 at room temp	0.45	$5.8/5.7 \times 10^{12} \pm 0.2/0.3 \times 10^{12}$	0.75/0.72	2.4/2.4	84.4	0.25/0.26
after 30 min in O_2 at 400 °C	0.2	$6.5 \times 10^{11} \pm 0.5 \times 10^{11}$	1.3	3.5	84.0	0.09
after 30 min in air at 400 °C	0.2	$1.3 \times 10^{12} \pm 0.2 \times 10^{12}$	1.1	2.5	84.0	0.09
after subsequent 45 min in H_2 at 200 °C	0.2	$1.3 \times 10^{12} \pm 0.1 \times 10^{12}$	1.1	2.5	84.0	0.09

[a] The mean width was calculated from the measured particle densities, mean heights, and the known coverage assuming spherical segment shaped gold particles.

TABLE 2: Change in Binding Energy and Relative Intensity of the Au(4f) Peak upon Room Temperature Exposure of a 0.1 ML Au Covered Au/TiO_2 Sample to O_2 (72 h, 50 mbar) and to Air (48 h, 1 bar)

sample	BE (eV) Au(4f)	relative intensity Au(4f)/Ti(2p)
after evaporation	84.4	0.07
after 72 h in 50 mbar O_2	84.4	0.07
after subsequent 48 h in 1 bar air	84.3/85.7	0.05

increased slightly (0.47 nm). These morphology changes are accompanied by a shift of the Au(4f) binding energy from 84.4 to 84.1 eV.

Comparing our results with data published previously, we find clear effects of the oxidation state of the surface and surface near regions on the thermal stability of the Au nanoparticles under UHV conditions. On a highly reduced, (1×2) reconstructed substrate, obtained by cycles of sputtering and annealing in UHV to 580 °C, significant particle growth and a decay in the particle density, by a factor of 20, were observed by STM after flash annealing to 500 °C,[20] which can be compared with the decay by 15% observed in our experiments upon annealing at 500 °C (30 min). On bulk reduced TiO_2(110) samples with reoxidized (1×1) surface particle growth was found to be slow[5,15] or negligible[6,14] at 400 °C, with small differences depending on the exact surface preparation. Significant sintering could be observed by STM only for higher annealing temperatures (625 °C, 1 h) or for long-term annealing at 475 °C (7 h).[15] On the other hand, a temperature-dependent LEIS study revealed first indications for sintering under UHV conditions already at 230 °C.[44]

Exposing the Au/TiO_2 model systems to 50 mbar O_2 at room temperature and reactive annealing in this atmosphere leads to partly different results compared to the corresponding UHV treatment. After room-temperature exposure to O_2, even for a very long time (72 h), we see no changes in the intensity or the BE of the Au(4f) peak of a 0.1 ML Au covered sample (see Figure 6 and Table 2). Hence, within the sensitivity of the XPS measurement room-temperature O_2 exposure is not sufficient to induce particle growth. Comparable results were obtained for a 0.45 ML Au covered sample (Figure 7). After 2 h exposure to 50 mbar O_2 the particle density was practically constant at 5.8×10^{12} particles·cm^{-2} (Figure 7a,b, compare also Figure 4b before O_2 exposure). Likewise the Au(4f)/Ti(2p) intensity ratio remained at 0.25, with a Au(4f) binding energy of 84.4 eV. Also after additional 13.5 h room-temperature exposure to 50 mbar O_2 we saw no significant changes, neither in the particle density (5.7×10^{12} particles·cm^{-2}) nor in the Au(4f)/Ti(2p) intensity ratio (0.26) or in the Au(4f) binding energy.

These results can be compared with previous results: Sykes et al. found significant particle sintering on polycrystalline TiO_2 films upon prolonged O_2 exposure (18 h, 1 bar), increasing the mean particle size from 2.4 to 4 nm.[23] The Au particles were found to migrate and agglomerate to grain boundaries. Lai and Goodman reported that the density of the Au clusters were greatly reduced and their size increased upon exposure to 13 mbar O_2 (120 min).[10] The Au particle growth was found to be size dependent, with particles >4 nm not being affected by room-temperature O_2 exposure.[10] In a subsequent paper from the same group,[9] however, the authors saw no change in the AES Au signal upon O_2 exposure and therefore favored an interpretation according to which the changes in the STM image upon room-temperature exposure to O_2 are due to an O_2 induced modification of the TiO_2(110) substrate already at room temperature.[9] Such modifications were indeed observed both on pure TiO_2(110)[7,21] and on Au/TiO_2(110).[9] Our results, which show practically no modifications of the Au particle size/density under exposure to 50 mbar O_2, agree with the latter interpretation. It may well be that at the much higher partial pressures used in ref 23 (1 bar O_2) the situation is different.

For comparison with previous STM studies we performed similar AFM/XPS experiments (2 h, 13.5 h room-temperature exposure to 50 mbar O_2) also on samples prepared on UHV annealed 'reduced' TiO_2(110) substrates. These showed a lower absolute value of the particle density (ca. 2.9×10^{12} cm^{-2}), but otherwise a rather similar morphology to those in Figures 4 and 7. The decrease in island density upon O_2 exposure is slightly higher than on the fully oxidized substrates, from 2.9×10^{12} to 2.5×10^{12} cm^{-2}; the difference to the fully oxidized samples, however, is rather small. This is different from previous findings for Ag/TiO_2(110), where significant effects of the chemical state of the substrate surface finally were reported.[10] Ripening in O_2 was much more pronounced on a reduced TiO_2-(110) substrate than on a substrate that had been exposed to O_2 before Ag deposition,[10] which was explained by the authors by a less efficient O_2 adsorption (and dissociation) on the reoxidized surface than on the reduced substrate. Activation of molecularly adsorbed O_2 on surface defects, specifically on O vacancies, had been reported in experimental and theoretical studies (see ref 21 and references therein), and these vacancies had also been reported to stabilize small Au clusters of a few atoms size.[45]

The activity for sintering is very different for reactive annealing at 400 °C in O_2 (30 min). Using a 0.2 ML Au covered sample, significant changes can be observed, both in the particle density and in the particle sizes (see Figure 8a,c). The particle distribution is still homogeneous, but the density decreases to 6.5×10^{11} cm^{-2}. The mean particle height/diameter is now 1.3/3.5 nm, the particle size distribution is shown in Figure 8e. The

TABLE 3: Au Particle Densities upon Deposition on TiO_2(110) Substrates Reported in Previous Studies

Au/TiO_2 model system	substrate preparation	deposition conditions	Au coverage (ML)	particle density (cm^{-2})	ref
Au/TiO_2(110) reduced + reoxidized (1 × 1) structure	sputter + anneal in O_2 (1000 K/5 × 10^{-7} mbar) cycles	evaporation at 300 K (0.21 ML/min)	0.08 0.2	3.8×10^{12} to 4.2×10^{12}	14
Au/TiO_2(110) reduced + reoxidized (1 × 1) structure	sputter + anneal (1100 K/UHV) cycles	evaporation at 300 K	0.25 1.0	2.7×10^{12} to 4.0×10^{12}	6, 10
Au/TiO_2(110) reduced + reoxidized (1 × 1) structure	sputter (0.8 keV) anneal (1100 K) cycles	evaporation at 300 K (0.18 ML/min)	0.2 0.8	1.8×10^{12} to 2.5×10^{12}	11, 19
Au/TiO_2(110) reduced, (1 × 2) reconstructed	sputter (3 keV) anneal (850 K) cycles	evaporation at 300 K	not mentioned	$\sim 4 \times 10^{12}$	20

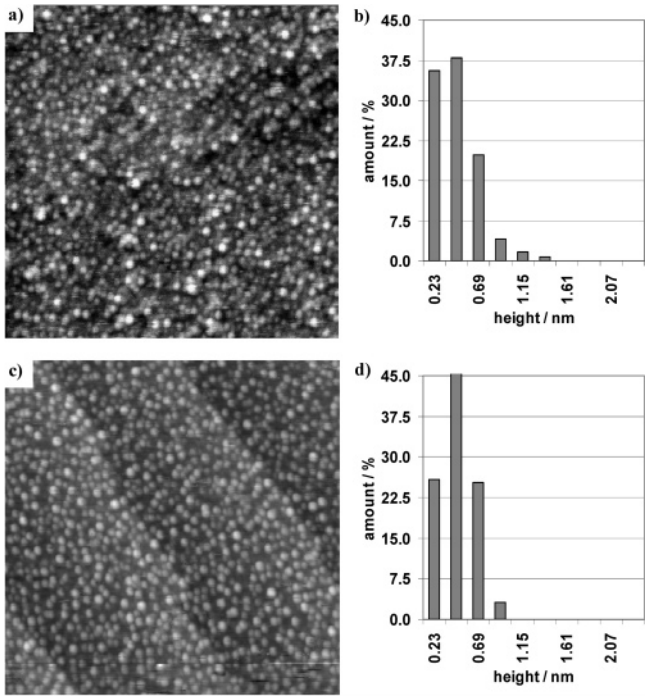

Figure 5. Nc-AFM images (a, c) of 0.2 ML Au on TiO_2 and particle height distributions (b, d) after annealing to (a, b) 400 °C and (c, d) 500 °C in UHV (175 nm × 175 nm)

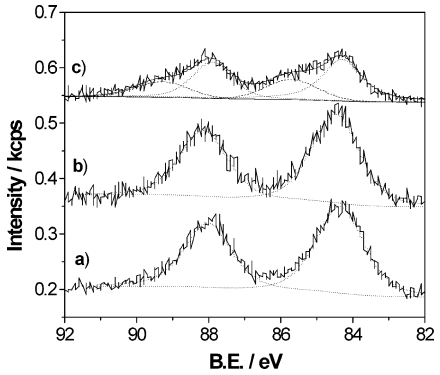

Figure 6. Comparison of the Au(4f) peaks of a Au/TiO_2 sample containing 0.1 ML Au: (a) after evaporation; (b) after exposure to oxygen; (c) after additional exposure to air.

Au(4f) peak intensity decreases and its position is shifted to the bulk gold value of 84.0 eV. These results emphasize the pronounced effect of oxygen on the Au particle growth. Hence, the thermal stability of small Au particles is significantly reduced in the presence of O_2.

Again, a different behavior is found when exposing a Au/TiO_2 model system to air at atmospheric pressure. The same 0.1 ML Au/TiO_2(110) sample that was stable for 72 h exposure to O_2 exhibits significant changes in the XPS data after exposure to air for 48 h at room temperature. Although the position of the main Au(4f) peak remains nearly constant, with a shift from

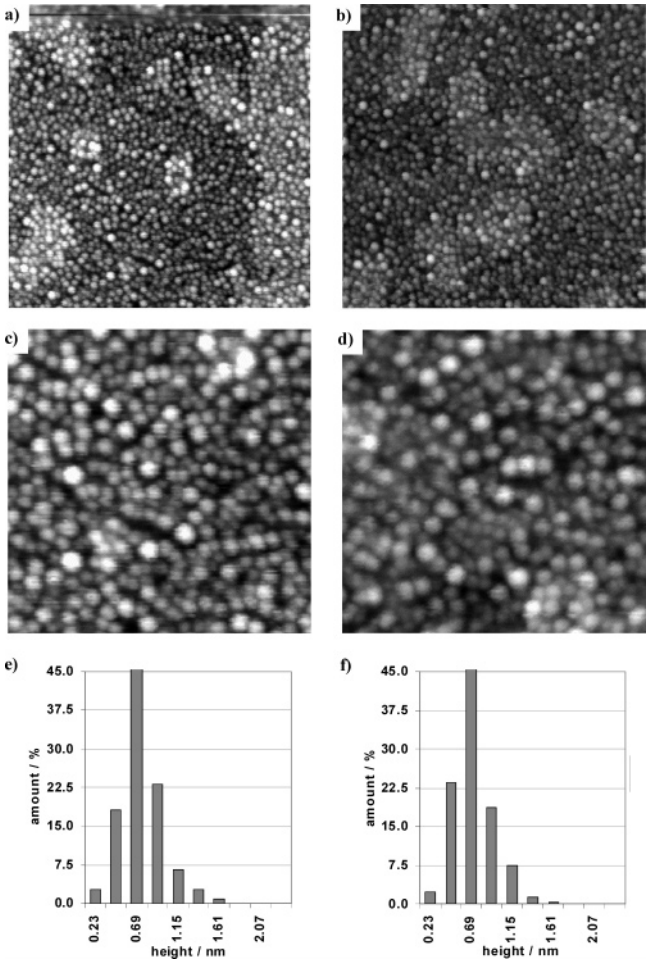

Figure 7. nc-AFM images (a−d) of 0.45 ML Au on TiO_2(110) and particle height distributions (e, f) after 2 h (a, c, e) and after additional 13.5 h (b, d, f) room-temperature exposure to 50 mbar O_2: (a, b) overview images, 160 × 160 nm; (c, d) higher resolution images, 70 nm × 70 nm.

84.4 to 84.3 eV (see Figure 6 and Table 2), a second Au(4f) peak at 85.7 eV appears in the spectrum, which is attributed to a Au−OH species.[46] The ratio of the peak intensities between Au^0 and Au−OH is approximately 2:1, indicating that a significant amount of the gold is hydroxylized after the exposure to air. Furthermore, the Au(4f)/Ti(2p) peak intensity ratio decreases by almost 30%. This indicates that a smaller fraction of the oxide surface is covered by Au now. Because evaporation from the surface can be excluded at room temperature, the growth of the gold particles is the only explanation for these results.

The results are different if the Au/TiO_2 model system (here 0.2 ML Au) is annealed for 30 min in 400 °C in air (see Figure 8b,d and Table 1). Now, we obtain a particle density of 1.3×10^{-12} cm^{-2} (particle size distribution in Figure 7f), which is significantly less than after UHV annealing, though by a factor of 2 more than after 50 mbar O_2 annealing of a similar sample

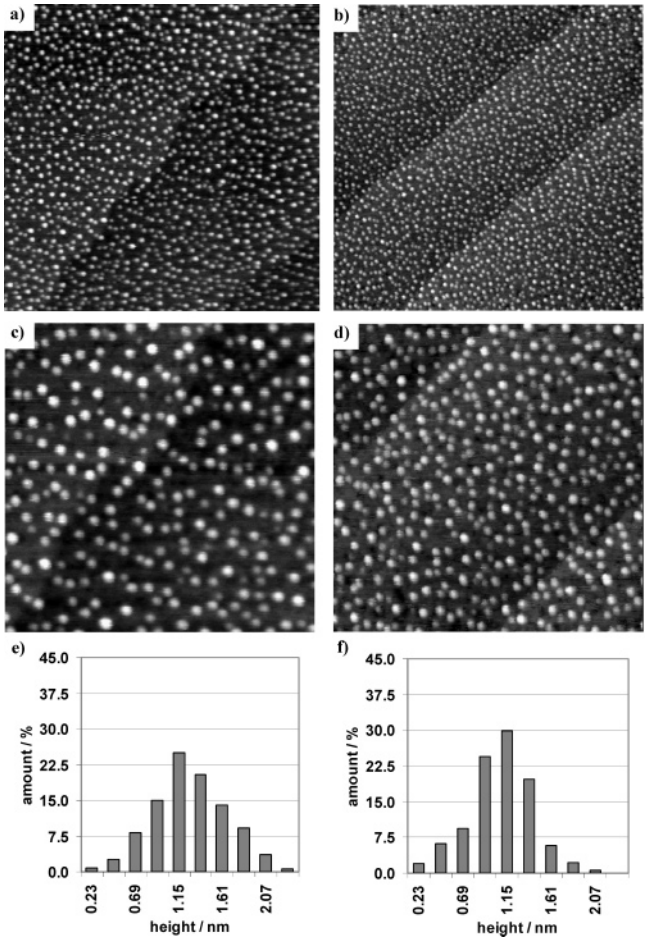

Figure 8. nc-AFM images (a−d) of 0.2 ML Au on TiO_2(110) and particle height distributions (e, f) after 30 min annealing at 400 °C in 50 mbar O_2 (a, c, e) or 1 bar air (b, d, f): (a, b) overview images, 400 nm × 400 nm; (c, d) higher resolution images, 175 nm × 175 nm.

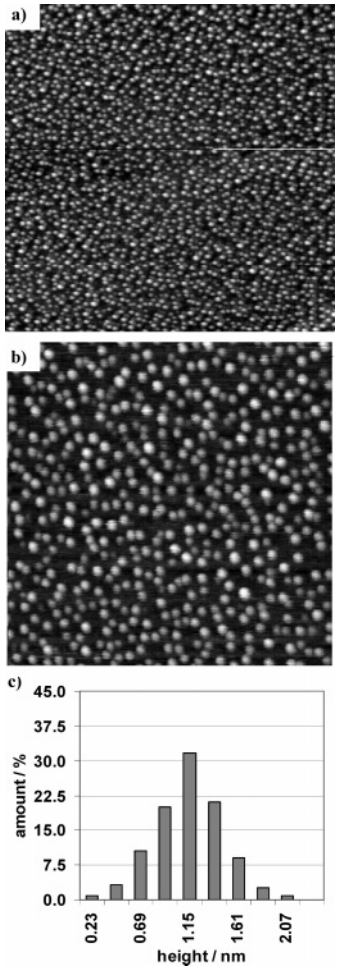

Figure 9. nc-AFM images (a, b) of 0.2 ML Au on TiO_2(110) and particle height distribution (c) after 30 min annealing at 400 °C in 1 bar air and subsequent 45 min annealing in 100 mbar H_2: (a) overview image, 400 nm × 400 nm; (b) higher resolution image, 175 nm × 175 nm.

at 400 °C. Because of the different experimental procedures for O_2 annealing and annealing in air, in the high-pressure cell and in an open oven, respectively, we consider the results in the two reactive atmospheres as rather similar. In both cases no Au−OH or AuO_x species can be found by XPS on these samples.

A significant particle growth upon prolonged room-temperature exposure to air was reported also for Au nanoparticles on polycrystalline TiO_2 films.[23] Furthermore, these authors reported migration even of 20 nm particles to grain boundaries, indicating a significant effective mobility also of these larger particles under ambient conditions, and concluded that interaction with water plays a role in the latter process. Our results, where the differences between room-temperature exposure to pure O_2 and to air are much more pronounced, support the conclusion that other components present in air, most likely water, affect the particle stability and growth. The presence of water can lead to the formation of hydroxides on the TiO_2 surface[21,47] which in turn may influence the particle stability. Second, the interaction of water or fragments resulting upon water adsorption may also directly facilitate gold particle growth via the formation of adsorbate stabilized gold adatoms, as was observed on a stepped Au(111) surface exposed to air.[48] This assumption is supported by the Au(4f) peak at 85.7 eV, which indicates that part of the gold surface atoms have reacted with adsorbed OH groups after the exposure to air and this may also contribute to the room-temperature cluster growth, which was not observed in pure oxygen.

At higher temperatures, e.g., 400 °C, adsorbed water and hydroxyl groups are desorbed or, at least partly, decomposed. The similarity to the annealing experiment in pure oxygen lets us suggest that under these conditions particle growth is, like in the latter experiment, dominated by the interaction with oxygen. In none of the different reactive annealing treatments did we find any indication of the development of a bimodal particle size distribution, as had been observed upon O_2 exposure of Ag/TiO_2(110).[9]

Finally we tested the stability of the 400 °C air annealed Au/TiO_2(110) samples upon a subsequent reductive treatment, by annealing in pure H_2 (100 mbar, 45 min) at 200 °C, which corresponds to the reductive treatments sometimes used for conditioning of disperse Au/TiO_2 catalysts.[26] As shown in the AFM images in Figure 9 and in Table 1 the density and mean size of the Au nanoparticles are hardly affected by this treatment. The same result is obtained also from XP spectra, which show no change in the relative Au(4f) intensity or in the Au(4f) binding energy. Considering the much higher temperature in the preceding oxidation step and the reduced stability of the Au nanoparticles in an O_2 atmosphere, this result fully agrees with expectations.

Using planar Au/TiO_2(110) model systems with fully stoichiometric TiO_2(110) substrates which are chemically identical to those in disperse Au/TiO_2 catalysts and with Au particle sizes which closely resemble those in realistic catalysts (2−3 nm)

we have found that reactive annealing in O_2 or in air under conditions typical for the pretreatment of realistic Au/TiO_2 catalysts leads to a significant decrease in particle density and increase in particle size. In contrast, exposure to O_2 at room temperature, 400 °C annealing under UHV conditions, or subsequent annealing in H_2 (200 °C) have little effect on the Au nanoparticles. These results fully agree with observations on disperse supported catalyst, where calcining at 400 °C was found to induce a significant particle growth, to about 2.5−3 nm particle size, which had prompted a search for milder conditioning procedures (see ref 26 and references therein). They also agree with the observation that a subsequent reductive annealing (200 °C) of the catalyst in a H_2 atmosphere, after calcination, has little effect on the particle size.[26] Finally, comparison with data presented by Goodman and co-workers[11] leads to the conclusion that the exposure to a CO/O_2 reaction atmosphere has much stronger effects on the Au nanoparticle stability and sintering at lower temperatures than exposure to pure (50 mbar) or diluted O_2. This explains observations in our laboratory that the higher activities of Au/TiO_2 catalysts for CO oxidation obtained after lower pretreatment temperatures, e.g., by going from 400 °C to 200 °C calcination temperature, are at least partly compensated by a faster deactivation of the latter catalysts (see also ref 26). In the reaction atmosphere, growth of the smaller Au nanoparticles is possible even at 80 °C reaction temperature, despite the preceding reactive annealing in a O_2 atmosphere at the still much higher temperature of 200 °C.

4. Summary

The thermal stability of Au nanoparticles on fully oxidized, stoichiometric $TiO_2(110)$ rutile single-crystal surfaces in UHV or in reactive atmospheres (50 mbar O_2 or 1 bar air) was investigated by combined AFM and XPS measurements. After evaporation of 0.2−1.0 ML Au, flat gold particles (height 0.2−0.6 nm, diameter 2.5−4 nm) are formed on the surface, which are randomly distributed with a particle density of about 4×10^{12} cm^{-2}. UHV annealing at 400 °C has little effect on the Au particle density/size for particles of these sizes, annealing at 500 °C leads to a measurable decay of the island density (−20%) and a corresponding increase of the particle size. Similar experiments in 50 mbar O_2 show that Au nanoparticles are rather stable at room temperature, whereas significant growth was observed upon annealing at 400 °C. Subsequent annealing in H_2 (200 °C) has no effect on the morphology of the Au/TiO_2-(110) interface. In 1 bar air, the gold particles are less stable and growth starts already at room temperature. The results show that oxygen has a pronounced effect on the growth of Au nanoparticles only at elevated temperatures, whereas at room temperature the influence of oxygen on the stability and growth of Au nanoparticles on $TiO_2(110)$ is small, both for partly reduced and fully oxidized $TiO_2(110)$ substrates. The results fully agree with observations on disperse supported Au/TiO_2 catalysts and allow a better understanding of the pretreatment procedures used for these catalysts.

Acknowledgment. This work was supported by the Deutsche Forschungsgemeinschaft, via Sonderforschungsbereich 569 and via project Be 1201/9-2, and by the Landesstiftung Baden-Württemberg (Competence Network Functional Nanostructures).

References and Notes

(1) Haruta, M.; Tsubota, S.; Kobayashi, T.; Kageyama, H.; Genet, M. J. Delmon, B. *J. Catal.* **1993**, *144*, 175.
(2) Haruta, M. *Catal. Surv. Jap*. **1997**, *1*, 61.
(3) Haruta, M. *CATECH* **2002**, *6*, 102.
(4) Bamwenda, G. R.; Tsubota, S.; Nakamura, T.; Haruta, M. *Catal. Lett*. **1997**, *44*, 83.
(5) Zhang, L.; Persaud, R.; Madey, T. E. *Phys. Rev*. B **1997**, *56*, 10549.
(6) Lai, X.; St. Clair, T. P.; Valden, M.; Goodmann, D. W. *Prog. Surf. Sci*. **1998**, *59*, 25.
(7) Valden, M.; Lai, X.; Goodman, D. W. *Science* **1998**, *281*, 1647.
(8) Parker, S. C.; Grant, A. W.; Bondzie, V. A.; Campbell, C. T. *Surf. Sci.* **1999**, *441*, 10.
(9) Kolmakov, A.; Goodman, D. W. *Catal. Lett*. **2000**, *70*, 93.
(10) Lai, X.; Goodman, D. W. *J. Mol. Catal. A* **2000**, *162*, 33.
(11) Kolmakov, A.; Goodman, D. W. *Surf. Sci*. **2001**, *490*, L597.
(12) Cosandey, F.; Zhang, L.; Madey, T. E. *Surf. Sci*. **2001**, *474*, 1.
(13) Cosandey, F.; Madey, T. E. *Surf. Rev. Lett*. **2001**, *8*, 73.
(14) Spiridis, N.; Haber, J.; Korecki, J. *Vacuum* **2001**, *63*, 99.
(15) Mitchell, C. E. J.; Howard, A.; Carney, M.; Egdell, R. G. *Surf. Sci*. **2001**, *490*, 196.
(16) Chusuei, C. C.; Lai, K.; Davis, K. A.; Bowers, E. K.; Fackler, J. P.; Goodman, D. W. *Langmuir* **2001**, *17*, 4113.
(17) Chusuei, C. C.; Lai, X.; Luo, K.; Goodmann, D. W. *Top. Catal*. **2001**, *14*, 1.
(18) Howard, A.; Clark, D. N. S.; Mitchell, C. E. J.; Egdell, R. G.; Dhanak, V. R. *Surf. Sci*. **2002**, *518*, 210.
(19) Kolmakov, A.; Goodman, D. W. *Chem. Record* **2002**, *2*, 446.
(20) Kitchin; J. R.; and Barteau, M. A. *Surf. Sci*. **2003**, *526*, 323.
(21) Diebold, U. *Surf. Sci. Rep*. **2003**, *48*, 53.
(22) Xu, C.; Oh, W. S.; Liu, G.; Kim, D. Y.; and Goodman, D. W. *J. Vac. Sci. Technol. A* **1997**, *15*, 1261.
(23) Sykes, E. C.; Williams, F. J.; Tikhov, M. S.; Lambert, R. M. *J. Phys. Chem. B* **2002**, *106*, 5930.
(24) Liu, Z. M.; Vannice, M. A. *Catal. Lett*. **1997**, *43*, 51.
(25) Valden, M.; Pak, S.; Lai, X.; Goodman, D. W. *Catal. Lett.* **1998**, *56*, 7.
(26) Schumacher, B.; Plzak, V.; Kinne, M.; Behm, R. J. *Catal. Lett*. **2003**, *89*, 109.
(27) Szabo, A.; Engel, T. *Surf. Sci.* **1995**, *329*, 241.
(28) Diebold, U.; Anderson, F.; Ng, K.-O.; Vanderbilt, D. *Phys. Rev. Lett*. **1998**, *77*, 1322.
(29) Sander, M.; Engel, T. *Surf. Sci*. **1994**, *302*, L263.
(30) Wiechers, J. Ph.D. Thesis, Ludwig-Maximilian-University Munich 1993.
(31) Borg, H. J.; van den Oetelaar, L. C. A.; van Itzendoorn, L. J.; Niemantsverdriet, J. W. *J. Vac. Sci. Technol. A* **1992**, *10*, 2737.
(32) Kuipers, H. P. C. E.; van Leuven, H. C. E.; Visser, W. M. *Surf. Interface Anal*. **1986**, *8*, 235.
(33) Aizawa, M.; Anderson, S. L. *J. Chem. Phys*. **2002**, *117*, 5001.
(34) Gonbeau, D.; Guimon, C.; Pfister-Guillouzo, G.; Levasseur, A.; Meunier, G.; Dormoy, R. *Surf. Sci.* **1991**, *254*, 81.
(35) Berkó, A.; Solymosi, F. *Langmuir* **1996**, *12*, 1257.
(36) Batzill, M.; Katsiev, K.; Gaspar, D. J.; Diebold, U. *Phys. Rev. B* **2002**, *66*, 235401−235401/10.
(37) Jak, M. J. J.; van Kreuningen, A.; Verhoeven, J.; Frenken, J. W. M. *Appl. Surf. Sci*. **2004**, *201*, 161.
(38) Nörenberg, H.; Tanner, R. E.; Schierbaum, K. D.; Fischer, S.; Briggs, G. A. D. *Surf. Sci.* **1998**, *396*, 52.
(39) Zhang, L. P.; Li, M.; Diebold, U. *Surf. Sci*. **1998**, *412/413*, 242.
(40) Akita, T.; Okumura, M.; Tanaka, K.; Haruta, M. *J. Catal*. **2002**, *212*, 119.
(41) Moulder, J. F.; Stickle, W. F.; Sobol, P. E.; Bomben, K. D. *Handbook of X-ray Photoelectron Spectroscopy*; Perkin-Elmer Corp.: Eden Prairie, MN, 1992.
(42) Wertheim, G. K.; DiCenzo, S. B.; Youngquist, S. E. *Phys. Rev. Lett.* **1983**, *51*, 2310.
(43) Yang, Z.; Wu, R. *Phys. Rev. B* **2003**, *67*, 81403.
(44) Campbell, C. T.; Parker, S. C.; Starr, D. E. *Science* **2002**, *298*, 811.
(45) Wahlström, E.; Lopez, N.; Schaub, R.; Thostrup, P.; Ronnau, A.; Africh, C.; Lagsgaard, E.; Norskov, J. K.; Besenbacher, F. *Phys. Rev. Lett*. **2003**, *90*, 261011.
(46) Pireaux, J.-J.; Liehr, M.; Thiry, P. A.; Delrue, J. P.; Caudano, R. *Surf. Sci*. **1984**, *141*, 221.
(47) Henderson, M. A. *Surf. Sci. Rep*. **2002**, *46*, 1.
(48) Peale, D. R.; Cooper, B. H. *J. Vac. Sci. Technol. A* **1992**, *10*, 2210.